Chemistry Europe
European Chemical
Societies Publishing

∎ **Silver Complexes** |*Hot Paper*|

Group 6 Hexacarbonyls as Ligands for the Silver Cation: Syntheses, Characterization, and Analysis of the Bonding Compared with the Isoelectronic Group 5 Hexacarbonylates

Jan Bohnenberger,[a] Daniel Kratzert,[a] Sai Manoj N. V. T. Gorantla,[b] Sudip Pan,[b] Gernot Frenking,*[b, c] and Ingo Krossing*[a]

Abstract: The syntheses of the two novel complexes $[Ag\{Mo/W(CO)_6\}_2]^+[F-\{Al(OR^F)_3\}_2]^-$ $(R^F = C(CF_3)_3)$ are reported along with their structural and spectroscopic characterization. The X-ray structure shows that three carbonyl ligands from each $M(CO)_6$ fragment bend towards the silver atom within binding Ag–C distance range. DFT calculations of the free cations $[Ag\{M(CO)_6\}_2]^+$ (M = Cr, Mo, W) in the electronic singlet state give equilibrium structures with C_2 symmetry with two bridging carbonyl groups from each hexacarbonyl ligand. Similar structures with C_2 symmetry (M = Nb) and D_2 symmetry (M = V, Ta) are calculated for the isoelectronic group 5 anions $[Ag\{M(CO)_6\}_2]^-$ (M = V, Nb, Ta). The electronic structure of the cations is analyzed with the QTAIM and EDA-NOCV methods, which provide detailed information about the nature of the chemical bonds between Ag^+ and the $\{M(CO)_6\}_2^q$ (q = −2, M = V, Nb, Ta; q = 0, M = Cr, Mo, W) ligands.

Introduction

Homoleptic carbonyl complexes as ligands for the silver ion Ag^+ are well known in the literature. Similar to homoleptic carbonyl complexes themselves, the variety of anionic clusters, with high nuclearity and formed from transition metal carbonylates like $[Fe(CO)_4]^{2-}$, is relatively large compared to that of neutral or cationic complexes. Thus, for anionic systems, examples from $[Ag_3\{Fe(CO)_4\}_3]^{3-[1]}$ to $[Ag_{13}\{Fe(CO)_4\}_8]^{4-[2]}$ and beyond are published. Most complexes of that kind are formally constructed from the respective homoleptic carbonyl anion $[M(CO)_x]^{y-}$ and a Ag^+ source. Thus, the large cluster anion $[Ag_9Os_{13}(CO)_{48}]^{-[3]}$ can be described as $[Ag_9\{Os_3(CO)_{11}\}_4\{Os(CO)_4\}]^-$ and $[Ag_{16}Ni_{24}(CO)_{40}]^{4-[4]}$ can be seen as $[Ag_{16}\{Ni_6(CO)_{10}\}_4]^{4-}$. Neutral species are scarce, the only known example resulted from the combination of Ag^+ and $[Co(CO)_4]^-$, giving a $\{AgCo(CO)_4\}_4$ tetramer.[5] The cationic members of this family of compounds were the last to be discovered. The $[Ag\{Fe(CO)_5\}_2]^+$ cation was the first, reported by us in 2014 and re-investigated by the Dias group in 2017.[6, 7] Interestingly, unlike its neutral or anionic relatives, it featured an, at that time, unprecedented coordination of a neutral carbonyl complex to a silver cation (Figure 1). We note that Ag^+ complexes with octahedral transition metal carbonyl units $[M(CO)_6]^x$ (x = −1, M = V, Nb, Ta; x = 0, M = Cr, Mo, W) are hitherto rather scarce and only in 2020 the first examples[8, 9] for any $[Ag_a\{M(CO)_6\}_b]^c$ units were published with M = Nb and Ta and the series of ions included with Figure 1.

Here, we describe syntheses towards the salts $[Ag\{M(CO)_6\}_2]^+[F-\{Al(OR^F)_3\}_2]^-$ (M = Mo, W), which include the first examples bearing a neutral hexacarbonyl ligand and their full electronic structure analysis including the recently published[9] isoelectronic, but negatively charged anions $[Ag\{M(CO)_6\}_2]^-$ (M = Nb, Ta) as $[NEt_4]^+$ salts.

Results and Discussion

Synthesis and characterization of $[Ag\{M(CO)_6\}_2][F-\{Al(OR^F)_3\}_2]$ (M = Mo, W)

During our continuous efforts to prepare novel transition metal carbonyl[10, 11] and nitrosyl[12, 13] cations as salts of the very good weakly coordinating anions[14] (WCAs) $[Al(OR^F)_4]^{-[15]}$ and
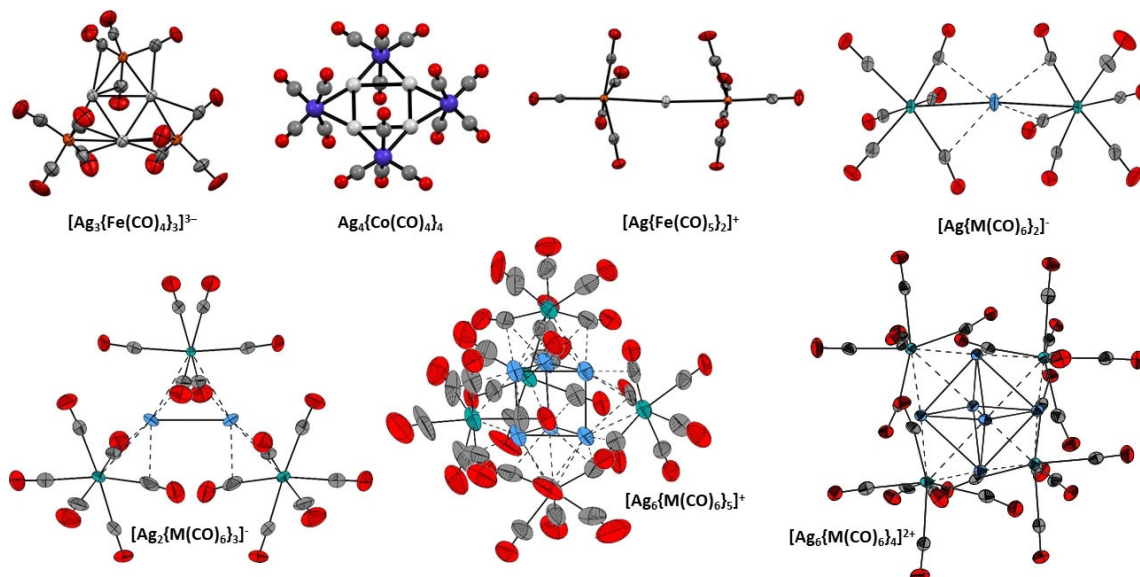
[a] Dr. J. Bohnenberger, Dr. D. Kratzert, Prof. Dr. I. Krossing
Institut für Anorganische und Analytische Chemie
Albert-Ludwigs-Universität Freiburg, Albertstrasse 21
79104 Freiburg (Germany)
E-mail: krossing@uni-freiburg.de

[b] S. M. N. V. T. Gorantla, Dr. S. Pan, Prof. Dr. G. Frenking
Fachbereich Chemie, Philipps-Universität Marburg
Hans-Meerwein-Straße, 35032 Marburg (Germany)
E-mail: frenking@chemie.uni-marburg.de

[c] Prof. Dr. G. Frenking
Institute of Advanced Synthesis, School of Chemistry and
Molecular Engineering, Jiangsu National Synergetic Innovation Center for
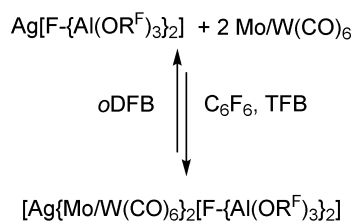Advanced Materials, Nanjing Tech University, Nanjing 211816 (P. R. China)

Chemistry–A European Journal

Full Paper
doi.org/10.1002/chem.202003934

**Chemistry
Europe**
European Chemical
Societies Publishing

Figure 1. Molecular structures of selected silver complexes with homoleptic carbonyl complexes as ligands, respective counterions omitted for clarity. Of special relevance are the recently published formal [M(CO)$_6$]$^-$ ligand (M=Nb and/or Ta) complexes, which include an isoelectronic ligand to the here targeted neutral M(CO)$_6$ ligands (M=Cr, Mo, W).

[F-{Al(OR^F)$_3$}$_2$]$^-$ (R^F = C(CF$_3$)$_3$),[16] we conducted experiments towards the synthesis of the homoleptic group 6 carbonyl radical cations [Mo(CO)$_6$]$^+$ and [W(CO)$_6$]$^+$.[17] An unsuccessful oxidation attempt of W(CO)$_6$ led to light-yellow crystals of [Ag{W(CO)$_6$}$_2$]$^+$ [F-{Al(OR^F)$_3$}$_2$]$^-$. The crystals readily decomposed to W(CO)$_6$ and [Ag(oDFB)$_x$]$^+$[F-{Al(OR^F)$_3$}$_2$]$^-$ upon dissolution in oDFB (=1,2-F$_2$C$_6$H$_4$, Scheme 1).

$$Ag[F-\{Al(OR^F)_3\}_2] + 2\ Mo/W(CO)_6$$

$$o\text{DFB} \big\Updownarrow C_6F_6,\ \text{TFB}$$

$$[Ag\{Mo/W(CO)_6\}_2[F-\{Al(OR^F)_3\}_2]$$

Scheme 1. Solvent dependence of the Mo/W(CO)$_6$ complexation reaction.

This explained why this species was never observed before: only the change to the even less coordinating solvents TFB (= 1,2,3,4-F$_4$C$_6$H$_2$) and C$_6$F$_6$—as also used for the very sensitive [W(CO)$_6$]$^+$ system[11,17]—made this discovery possible. This points out that the W(CO)$_6$ ligand is weakly bound.
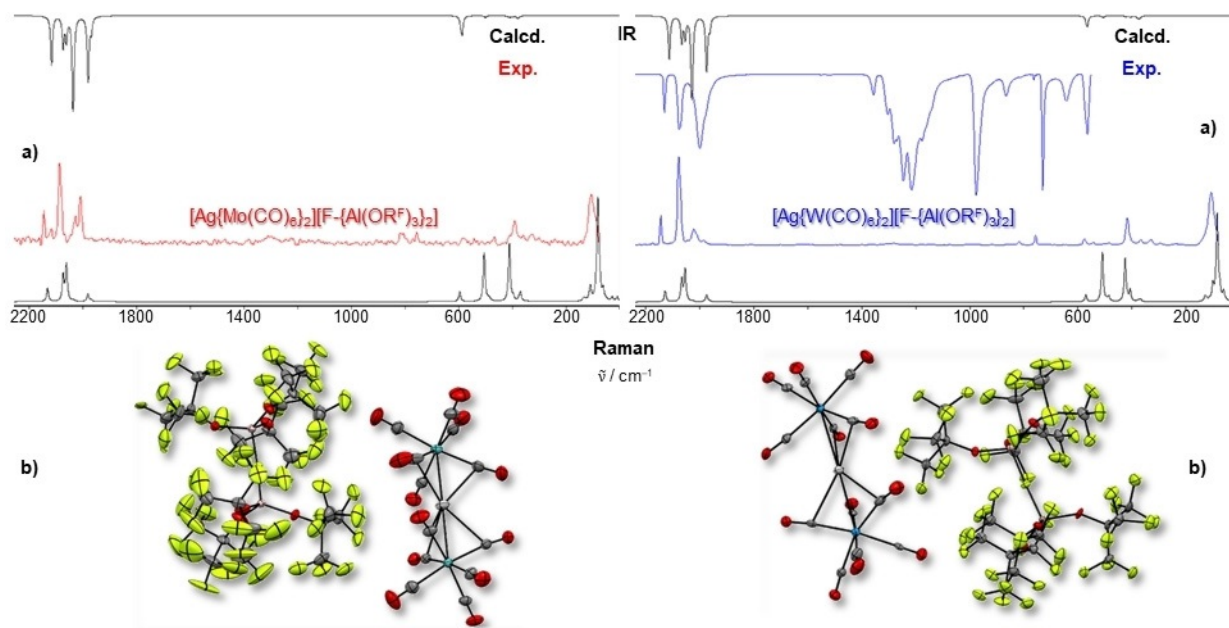
Directed synthesis

[Ag{W(CO)$_6$}$_2$]$^+$[F-{Al(OR^F)$_3$}$_2$]$^-$ can be selectively synthesized from Ag[F-{Al(OR^F)$_3$}$_2$][16] and two equivalents of W(CO)$_6$ in C$_6$F$_6$. A subsequent crystallization from TFB layered with n-pentane gave an 86 % yield of a crystalline material, which was shown by powder X-ray diffraction analysis to be the phase-pure product (Figure S2 in the Supporting Information). It seems likely that the synthesis also works when TFB is used as a sol-

vent altogether. The same method can also be applied to Mo(CO)$_6$ and yields colorless crystals of [Ag{Mo(CO)$_6$}$_2$]$^+$[F-{Al(OR^F)$_3$}$_2$]$^-$. This complex is even more sensitive and also decomposes upon contact with oDFB to solvated Ag$^+$ and the neutral carbonyl, but in addition it is unstable in substance. The colorless crystals turned dark overnight and the IR spectrum recorded the subsequent day showed, amongst other bands, CO stretching vibrations similar to those of [Mo(CO)$_6$]$^+$. This implies that [Mo(CO)$_6$]$^+$ can in principle be synthesized from Ag$^+$ in C$_6$F$_6$ or TFB without the need[17] of I$_2$ as the co-oxidant. All attempts to prepare a salt with the lighter chromium carbonyl [Ag{Cr(CO)$_6$}$_2$]$^+$ were futile in our hands.

Vibrational spectra

The measured vibrational spectra are in good agreement with the DFT calculations (Figure 2, top). The broadened bands in the IR spectrum of [Ag{W(CO)$_6$}$_2$]$^+$[F-{Al(OR^F)$_3$}$_2$]$^-$ suggest a flexible structure with lower local symmetry than the calculated C$_2$-symmetric gas-phase minimum structure. This also shows in the molecular structures, as the bonds of the two W(CO)$_6$ fragments to Ag$^+$ are similar, but not equal (see Figure 3 and Table 1). Remarkably, the calculations do not predict a difference in the M–CO bond lengths for terminal CO (CO$_{term}$) and CO ligands with contacts to the Ag atom (CO$_{Ag}$), whereas in the experimental structure the latter are shortened. On average, the experimental six Ag–C contacts are shorter for the Mo system than for W, which agrees with the calculations. Similar to the neutral M(CO)$_6$ species (cf. Mo(CO)$_6$: 205.9(4) pm,[18] W(CO)$_6$: 204.9(5) pm[19]), the experimental M–CO bonds are shorter for W (Table 1) unlike in the calculations. However, owing to the large standard deviations for the W structure as well as the 150 K data for the Mo system, these data should be interpreted with caution. For comparison, Table 1 includes the

Chemistry–A European Journal

Full Paper
doi.org/10.1002/chem.202003934

Chemistry Europe
European Chemical
Societies Publishing

Figure 2. Comparison of the experimental ([Ag{Mo(CO)$_6$}$_2$]$^+$[F-{Al(OR^F)$_3$}$_2$]$^-$, red, and [Ag{W(CO)$_6$}$_2$]$^+$[F-{Al(OR^F)$_3$}$_2$]$^-$, blue, and calculated (@BP86-D3BJ/def2-TZVPP, black) vibrational spectra (a) as well as their molecular structures (b). $P\bar{1}$, $R1 = 5.5\%$, $wR2 = 14.4\%$ and $P\bar{1}$, $R1 = 7.5\%$, $wR2 = 14.0\%$. Note: the IR spectrum of clean [Ag{Mo(CO)$_6$}$_2$]$^+$[F-{Al(OR^F)$_3$}$_2$]$^-$ could not be measured owing to its sensitivity; its crystal structure had to be measured at 150 K to solve the overstructure problems occurring at lower temperatures. Thermal ellipsoids are drawn at the 50% probability level.

[Ag{Mo(CO)$_6$}$_2$][F-{Al(OR^F)$_3$}$_2$]   **[Ag{W(CO)$_6$}$_2$][F-{Al(OR^F)$_3$}$_2$]**
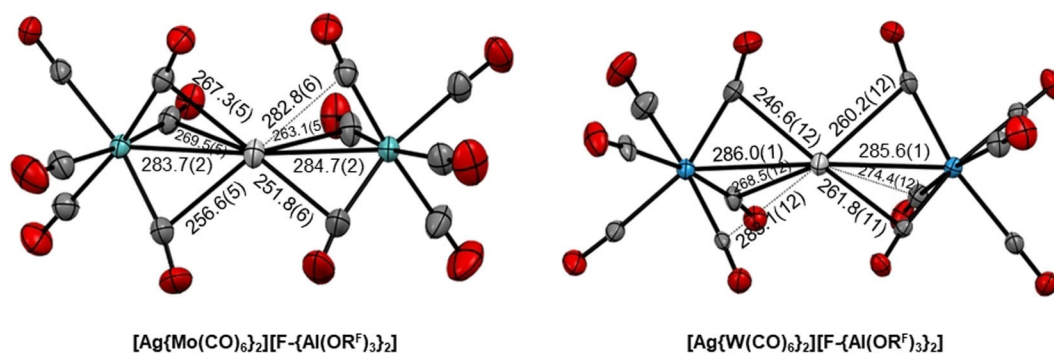
Figure 3. Detailed Ag bond lengths (in pm) of the cationic parts of [Ag{Mo(CO)$_6$}$_2$][F-{Al(OR^F)$_3$}$_2$] (left) and [Ag{W(CO)$_6$}$_2$][F-{Al(OR^F)$_3$}$_2$] (right).

spectroscopic and structural data of [Ag{Fe(CO)$_5$}$_2$]$^+$ [Al(OR^F)$_4$]$^-$.[7] The Raman spectra of [Ag{Mo(CO)$_6$}$_2$][F-{Al(OR^F)$_3$}$_2$] show only little differences in the energy of the CO vibrations between Mo and W, although the appearance of additional, rather IR active, bands for Mo suggest a distinct asymmetry in this complex as evident also from the molecular cation structure shown in more detail in Figure 3.

The experimental observations are also in accordance with the DFT-calculated thermodynamics of a possible reaction of the complexes M(CO)$_x$-Ag$^+$ with oDFB to the solvated Ag$^+$ and neutral carbonyl (Scheme 2). The gas-phase $\Delta_r H°_{gas}$ calculations show the same trend as the COSMO $\Delta_r G°_{solv}$ calculations in oDFB solution ($\varepsilon_r = 13.8$): [Ag{Fe(CO)$_5$}$_2$]$^+$ is the most stable complex and the only system for which the decomposition reaction with oDFB is disfavored by $+43$ kJ mol^{-1} (Scheme 2). The M(CO)$_6$ triad is, as observed, not stable in oDFB and the decomposition is thermodynamically favored. Also, the very

unfavorable thermodynamics for the formation of the hypothetical [Ag{Cr(CO)$_6$}$_2$]$^+$ is in agreement with our futile synthesis and isolation attempts.

Thus, the complex ions [Ag{M(CO)$_6$}$_2$]$^+$ with M = Mo and W are at the stability edge and for M = Cr, in our hands, was not accessible. This is in line with the fleeting stability of the isoelectronic complex ions in [NEt$_4$]$^+$[Ag{M(CO)$_6$}$_2$]$^-$ (M = Nb, Ta), which start to decompose around -15 °C.[9] For comparison, the bonding situation of both sets of ions will be compared in the next section.

Theoretical investigation of the bonding situation

Structure and bonding within [Ag{M(CO)$_6$}$_2$]$^+$ (M = Cr, Mo, W)

Optimized structures: We optimized the geometries of the group 6 hexacarbonyl complexes [Ag{M(CO)$_6$}$_2$]$^+$ (M = Cr, Mo, W) at the BP86-D3(BJ)/def2-TZVPP level of theory. The calcula-

	[Ag{Mo(CO)₆}₂]⁺ [F-{Al(ORᶠ)₃}₂]⁻	[Ag{Mo(CO)₆}₂]⁺ calcd[a]	[Ag{W(CO)₆}₂]⁺ [F-{Al(ORᶠ)₃}₂]⁻	[Ag{W(CO)₆}₂]⁺ calcd[a]	[Ag{Cr(CO)₆}₂]⁺ calcd[a]	Assignment	[Ag{Fe(CO)₅}₂]⁺-[Al(ORᶠ)₄]⁻[7]
$\tilde{\nu}$ (CO) IR [cm⁻¹]	_[b]	2113 (ms)	2129 (mw)	2111 (ms)	2109 (ms)	(B)	2137 (m)
		2070 (mw)	2074 (m)	2065 (mw)	2068 (m)	(B)	2080 (vs)
		2058 (mw)	1998 (s, br)	2052 (mw)	2057 (mw)	(A + B)	2068 (ms, sh)
		2033 (vvs)		2027 (vvs)	2037 (vvs)	(A + B)	2038 (s, br)
		1977 (s)		1973 (s)	1972 (s)	(A + B)	2028 (s, br)
		1966 (w)		1961 (w)	1960 (w)	(B)	
$\tilde{\nu}$ (CO) Raman [cm⁻¹]	2142 (m)	2128 (vvw)	2142 (mw)	2126 (vw)	2124 (vw)	(A)	2150 (s)
	2114 (w)	2070 (w)	2076 (vvs)	2065 (w)	2068 (w)	(A)	2099 (vs)
	2083 (vvw)	2058 (mw)	2044 (vvw)	2052 (mw)	2057 (w)	(A)	2072 (vs)
	2024 (mw)	2033 (vvs)	2020 (vvw)	2026 (vvw)	2037 (vvw)	(A + B)	
	2005 (s)	1977 (s)	1983 (vvw)	1973 (vw)	1975 (vvw)	(A + B)	
		1966 (w)		1961 (vvw)	1960 (vvw)	(B)	
$\tilde{\nu}$ (M−Ag) [cm⁻¹]	103 (ms)[c]	106 (vw)	102 (ms)[c]	96 (w)	177 (vvw)	(B)	
					123 (vw)	(A)	
d(M−CO) [pm][d]	209.0(5)term[e]	207.0term	207.6(13)term	208.2term	191.9term		184.9(5)term
	206.1(5)Ag	207.1Ag	205.5(13)Ag	208.2Ag	193.1Ag		183.0(4)Ag
d(Ag−CO) [pm]	251.8(6)[e]	241.4	246.6(12)	242.9	236.1		276.9(5)
	256.6(5)	242.2	260.2(12)	243.9	236.2		281.1(5)
	263.1(5)		261.8(11)				283.5(5)
	267.3(5)		268.6(12)				291.3(5)
	269.5(5)		274.4(12)				301.3(5)
	282.8(6)		283.1(12)				301.4(5)
	Avg.: 260.2(6)		Avg.: 265.8(12)				301.9(5)
							312.9(5)
d(M−Ag) [pm]	284.2(2)[e]	281.3	285.8(1)	283.0	272.7		259.8(1)
$\Delta_r H°_{gas}$/$\Delta_r G°_{solv}$ [kJ mol⁻¹][f]		−68/−10		−66/−7	−108/−46		−21/+43

Table 1. Comparison of the experimental and calculated (calcd, BP86-D3BJ/def2-TZVPP) metric data of the triad [Ag{Cr/Mo/W(CO)₆}₂][F-{Al(ORᶠ)₃}₂]; w: weak, m: medium, s: strong, v: very, br: broad, avg.: averaged.

[a] C_2 symmetry, no scaling factor was applied. [b] No reliable IR spectrum could be measured owing to decomposition. [c] The assignment of the M−Ag stretch vibration is ambiguous. [d] There are two sets of similar CO ligands: terminal (term) and with contacts to the silver atom (Ag), averaged distances are given for each set. [e] Crystal structure was measured at 150 K to solve the overstructure problems. [f] BP86-D3BJ/def2-TZVPP (COSMO) calculations for the reaction [Ag{M(CO)ₓ}₂]⁺ + 3 oDFB ⇌ [Ag(oDFB₃)]⁺ + 2 M(CO)ₓ in oDFB ($\varepsilon_r = 13.8$) for M = Cr, Mo, W (all $x = 6$), Fe ($x = 5$) in C_1 symmetry.

$$[Ag\{M(CO)_x\}_2]^+ \; + \; 3\,oDFB \;\rightleftharpoons\; [Ag(oDFB)_3]^+ \; + \; 2\,M(CO)_x$$

$$\Delta_r H°_{gas} \; / \; \Delta_r G°_{solv} \; (\text{kJ mol}^{-1})$$

$$M = \begin{array}{lcr} \text{Fe} & -21 & / & +43 \\ \text{Cr} & -108 & / & -46 \\ \text{Mo} & -68 & / & -10 \\ \text{W} & -66 & / & -7 \end{array}$$
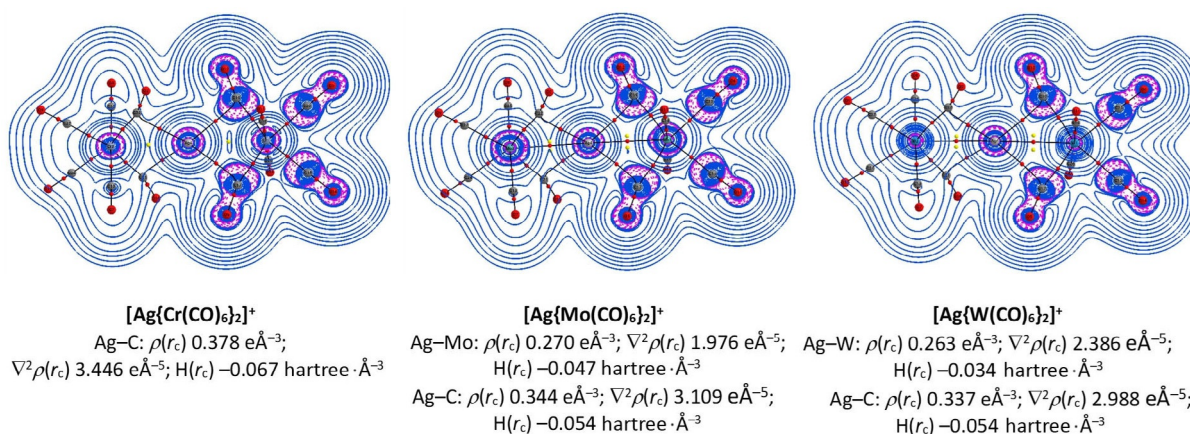
Scheme 2. BP86-D3BJ/def2-TZVPP (COSMO) thermodynamics.

tions give equilibrium structures with C_2 symmetry where two carbonyl groups of each {M(CO)₆} ligand are in a bridging position toward Ag⁺ (Figure S3 in the Supporting Information). The experimental structures of the M = Mo, W complexes exhibit three bridging CO groups each with significantly different Ag−CO bond lengths, which vary between 2.518–2.828 Å (Mo) and 2.466–2.861 Å (W), which are somewhat longer than the calculated Ag−CO distances. The other calculated bond lengths of the Mo and W adducts are in good agreement with the experimental values of the X-ray structure determination. The differences between theory and experiment concerning the bridging CO groups may be attributed to the effect of the counterion and solid-state forces. However, this will not affect the principle bonding analysis and the theoretical data was

therefore used for the bonding analysis of the free cations [Ag{M(CO)₆}₂]⁺ (M = Cr, Mo, W).

QTAIM analysis: We first carried out a QTAIM analysis[20] of the electronic structure of [Ag{M(CO)₆}₂]⁺ (M = Cr, Mo, W). Figure 4 shows the contour plots of the Laplacian of the electron density, $\nabla^2\rho(r)$ in the Ag-C-M plane, where C denotes the bridging carbonyl carbon atom of one {M(CO)₆}₂ moiety.

There are in all three systems bond paths between the silver atom and the four bridging carbonyl carbon atoms. There are also direct bond paths for the Ag−M interactions for M = Mo and W but not for M = Cr. The latter cation [Ag{Cr(CO)₆}₂]⁺ has instead a ring critical point in the center of the cyclic Ag-C-Cr-C fragment. This indicates a somewhat different bonding situation in the chromium complex than in the heavier group 6 homologues, which is a further example of the difference between the chemical bonds of 3d transition metals and their 4d and 5d homologues.[21] The appearance or non-appearance of a bond critical point (bcp) and bond path for the Ag−M interactions are not identified with a drastic change in the interatomic interactions or the occurrence or absence of a chemical bond.[22] This rather suggests subtle changes in the topography of the electronic structure in a static picture, which should be considered in conjunction with further information about the nature of the electronic structure. Yet, it is interesting to note

Chemistry–A European Journal

Full Paper

doi.org/10.1002/chem.202003934

Chemistry Europe
European Chemical
Societies Publishing

Figure 4. The contour plot of the Laplacian of electron density, $\nabla^2\rho(r)$ in the Ag-C-M plane of $[Ag\{M(CO)_6\}_2]^+$ (M = Cr, Mo, W). The values of topological descriptors are provided in atomic units (au). The blue solid lines indicate regions of charge depletion ($\nabla^2\rho(r) > 0$) and red dotted lines indicate regions of charge accumulation ($\nabla^2\rho(r) < 0$). Red and yellow spheres represent bond critical points and ring critical points, respectively.

that the charge densities residing on the Ag–C bcps are consistently higher than those on the existing Ag–M bcps.

EDA-NOCV analysis: We analyzed the bonding situation in $[Ag\{M(CO)_6\}_2]^+$ (M = Cr, Mo, W) with the EDA-NOCV method[23] focusing on the orbital interactions between Ag$^+$ and the $\{M(CO)_6\}_2$ ligands. Table 2 shows the numerical results of the calculations. As the large majority of EDA-NOCV work has hitherto been published using kcal mol^{-1} as units, we left our data with this convention. Note that the intrinsic attraction between Ag$^+$ and the metal hexacarbonyls has nearly equal strength for M = Mo and W (-86 kcal mol^{-1}), whereas for M = Cr it is weaker (-80 kcal mol^{-1}). This agrees with the experimental observation that the chromium complex is less stable than the heavier homologues.

The breakdown of the attractive interactions between Ag$^+$ and $\{M(CO)_6\}_2$ suggests that the electrostatic attraction ΔE_{elstat}

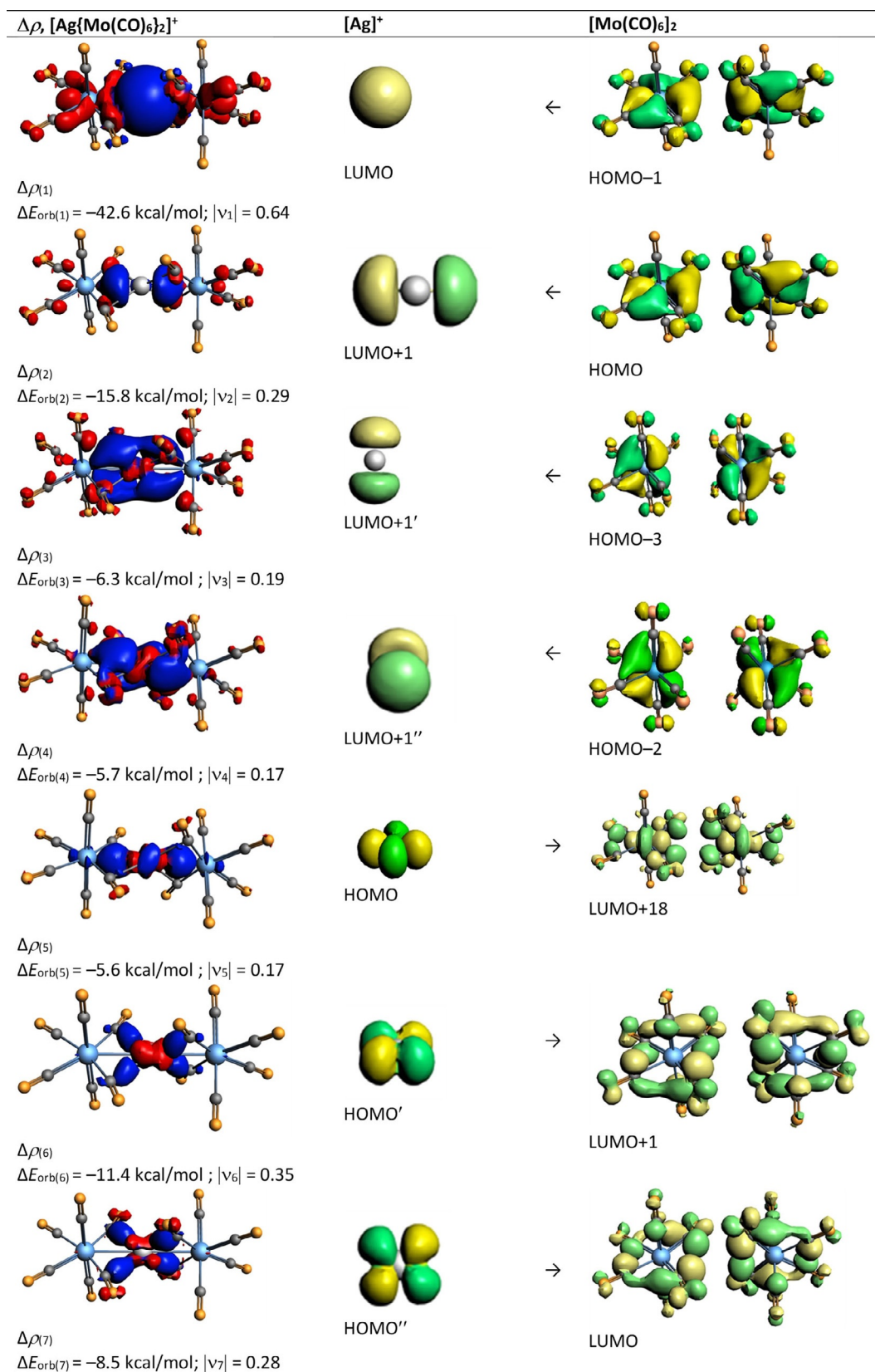and the orbital (covalent) interactions ΔE_{orb} have similar strength and that the dispersion forces are rather weak. Inspection of the orbital term identifies nine individual pairwise terms $\Delta E_{orb(1)}-\Delta E_{orb(9)}$, which can be attributed to the interactions between Ag$^+$ and $\{M(CO)_6\}_2$. The largest contributions come as expected from the donation of the ligand to the silver cation $[M(CO)_6]\rightarrow Ag^+\leftarrow[M(CO)_6]$, which provides 56–61% of ΔE_{orb}, but the backdonation $[M(CO)_6]\leftarrow Ag^+\rightarrow[M(CO)_6]$ is not negligible, accounting for 26–28% of the orbital interactions. The remaining part of the orbital stabilization is due to polarization within the ligand orbitals.

The individual orbital interactions $\Delta E_{orb(1)}-\Delta E_{orb(9)}$ can be identified by visual inspection of the associated deformation densities $\Delta\rho_{(1)}-\Delta\rho_{(9)}$. They are displayed in Figure 5 together with the connected most important fragment orbitals of the molybdenum complex $[Ag\{Mo(CO)_6\}_2]^+$. The deformation den-

Table 2. EDA-NOCV results for $[Ag\{M(CO)_6\}_2]^+$ (M = Cr, Mo, W) complexes using Ag$^+$ and $\{M(CO)_6\}_2$ as interacting fragments at the BP86-D3(BJ)/TZ2P level. Energy values are given in kcal mol^{-1}. Calculated partial charge q(Ag) given by the NBO method and (in parentheses) the eigenvalues of the orbital interactions (see Figure 4).

Energies	Orbital interaction	$[Ag]^+ + [Cr(CO)_6]_2$	$[Ag]^+ + [Mo(CO)_6]_2$	$[Ag]^+ + [W(CO)_6]_2$
ΔE_{int}		-79.8	-86.1	-86.7
ΔE_{Pauli}		158.3	151.2	151.0
ΔE_{disp}		-9.6 (4.0%)	-10.8 (4.6%)	-11.5 (4.8%)
ΔE_{elstat}[a]		-110.7 (46.5%)	-108.9 (45.9%)	-108.6 (45.7%)
ΔE_{orb}[a]		-117.8 (49.5%)	-117.6 (49.6%)	-117.6 (49.5%)
$\Delta E_{orb(1)}$[b]	$[TM(CO)_6]\rightarrow Ag^+(s)\leftarrow[TM(CO)_6]$ σ donation	-39.9 (33.9%)	-42.6 (36.2%)	-43.6 (37.1%)
$\Delta E_{orb(2)}$[b]	$[TM(CO)_6]\rightarrow Ag^+(p_\sigma)\leftarrow[TM(CO)_6]$ σ donation	-14.1 (12.0%)	-15.8 (13.4%)	-16.3 (13.9%)
$\Delta E_{orb(3)}$[b]	$[TM(CO)_6]\rightarrow Ag^+(p_\pi)\leftarrow[TM(CO)_6]$ π donation	-5.9 (5.0%)	-6.3 (5.4%)	-6.3 (5.4%)
$\Delta E_{orb(4)}$[b]	$[TM(CO)_6]\rightarrow Ag^+(p_\pi)\leftarrow[TM(CO)_6]$ π donation	-5.6 (4.8%)	-5.7 (4.8%)	-5.7 (4.8%)
$\Delta E_{orb(5)}$[b]	$[TM(CO)_6]\leftarrow Ag^+(d_\sigma)\rightarrow[TM(CO)_6]$ σ backdonation	-4.4 (3.7%)	-5.6 (4.8%)	-6.1 (5.2%)
$\Delta E_{orb(6)}$[b]	$[TM(CO)_6]\leftarrow Ag^+(d_\pi)\rightarrow[TM(CO)_6]$ π backdonation	-13.5 (11.5%)	-11.4 (9.7%)	-10.9 (9.3%)
$\Delta E_{orb(7)}$[b]	$[TM(CO)_6]\leftarrow Ag^+(d_\pi)\rightarrow[TM(CO)_6]$ π backdonation	-9.9 (8.4%)	-8.5 (7.2%)	-8.1 (6.9%)
$\Delta E_{orb(8)}$[b	$[TM(CO)_6]\leftarrow Ag^+(d_\sigma)\rightarrow[TM(CO)_6]$ σ backdonation	-4.6 (3.9%)	-4.3 (3.7%)	-4.1 (3.5%)
$\Delta E_{orb(9)}$[b]	$[TM(CO)_6]\leftarrow Ag^+(d_\delta)\rightarrow[TM(CO)_6]$ δ backdonation	-2.9 (2.5%)	-2.7 (2.3%)	-2.5 (2.1%)
$\Delta E_{orb(rest)}$[b]		-17.0 (14.4%)	-14.7 (12.5%)	-14.0 (11.9%)
q(Ag)		0.75 (0.89)	0.71 (0.81)	0.70 (0.82)

[a] The values in the parentheses show the contribution to the total attractive interaction $\Delta E_{elstat} + \Delta E_{orb} + \Delta E_{disp}$. [b] The values in parentheses show the contribution to the total orbital interaction ΔE_{orb}.

Chemistry–A European Journal

Full Paper
doi.org/10.1002/chem.202003934

Chemistry Europe
European Chemical
Societies Publishing

$\Delta\rho$, $[Ag\{Mo(CO)_6\}_2]^+$	$[Ag]^+$	$[Mo(CO)_6]_2$

$\Delta\rho_{(1)}$
$\Delta E_{orb(1)} = -42.6$ kcal/mol; $|\nu_1| = 0.64$

LUMO

HOMO−1

$\Delta\rho_{(2)}$
$\Delta E_{orb(2)} = -15.8$ kcal/mol; $|\nu_2| = 0.29$

LUMO+1

HOMO

$\Delta\rho_{(3)}$
$\Delta E_{orb(3)} = -6.3$ kcal/mol ; $|\nu_3| = 0.19$

LUMO+1′

HOMO−3

$\Delta\rho_{(4)}$
$\Delta E_{orb(4)} = -5.7$ kcal/mol ; $|\nu_4| = 0.17$

LUMO+1″

HOMO−2

$\Delta\rho_{(5)}$
$\Delta E_{orb(5)} = -5.6$ kcal/mol ; $|\nu_5| = 0.17$

HOMO

LUMO+18

$\Delta\rho_{(6)}$
$\Delta E_{orb(6)} = -11.4$ kcal/mol ; $|\nu_6| = 0.35$

HOMO′

LUMO+1

$\Delta\rho_{(7)}$
$\Delta E_{orb(7)} = -8.5$ kcal/mol; $|\nu_7| = 0.28$

HOMO″

LUMO

Figure 5. The shape of the deformation densities $\Delta\rho_{(1)-(7)}$ that correspond to $\Delta E_{orb(1)-(7)}$, and the fragments orbitals of $[Ag]^+$ and $[Mo(CO)_6]_2$ in the singlet state at the BP86-D3(BJ)/TZ2P level. Isosurface values are 0.001 au. The eigenvalues $|\nu_n|$ give the size of the charge migration in e. The direction of the charge flow of the deformation densities is red→blue.

Chemistry–A European Journal

Full Paper
doi.org/10.1002/chem.202003934

Chemistry Europe
European Chemical
Societies Publishing

sities $\Delta\rho_{(1)}-\Delta\rho_{(9)}$ and the fragment orbitals of the chromium and tungsten complexes look very similar and are shown in Figures S4 and S5 in the Supporting Information. The four terms $\Delta E_{orb(1)}-\Delta E_{orb(4)}$ for $[M(CO)_6]\rightarrow Ag^+\leftarrow[M(CO)_6]$ donation comprise σ donation into the 5s atomic orbital (AO) ($\Delta E_{orb(1)}$) and the 4p(σ) AO of Ag^+ ($\Delta E_{orb(2)}$) and weaker π donation into the 5p(π) AOs ($\Delta E_{orb(3)/(4)}$). The significant involvement of the 5p AOs of Ag^+ is remarkable, because the natural bond orbital (NBO) method does not consider the (n)p AOs of the transition metal as genuine valence orbitals.[24] The five terms $[M(CO)_6]\leftarrow Ag^+\rightarrow[M(CO)_6]$ can likewise be attributed to the σ, π, and δ backdonation from filled 4d AOs of Ag^+ to vacant ligand molecular orbitals (MOs). Inspection of the occupied and vacant orbitals of the $[M(CO)_6]$ ligands shows that the donation $[M(CO)_6]\rightarrow Ag^+\leftarrow[M(CO)_6]$ involves occupied orbitals that have the largest coefficients at the metal atom M. In contrast, the backdonation $[M(CO)_6]\leftarrow Ag^+\rightarrow[M(CO)_6]$ donates charge into pure CO π* orbitals ($\Delta E_{orb(6)}$, $\Delta E_{orb(7)}$, $\Delta E_{orb(9)}$) but also into antibonding combinations of metal AOs and CO orbitals ($\Delta E_{orb(5)}$, $\Delta E_{orb(8)}$). The eigenvalues $|v_n|$ of the donation and backdonation, which indicate the size of the charge migration in $[Ag\{M(CO)_6\}_2]^+$, suggest that the partial charge of the silver atom in the complexes is between $+0.81$ e (M = Mo) and $+0.89$ e (M = Cr), which nicely agree with the NBO charges (Table 2).
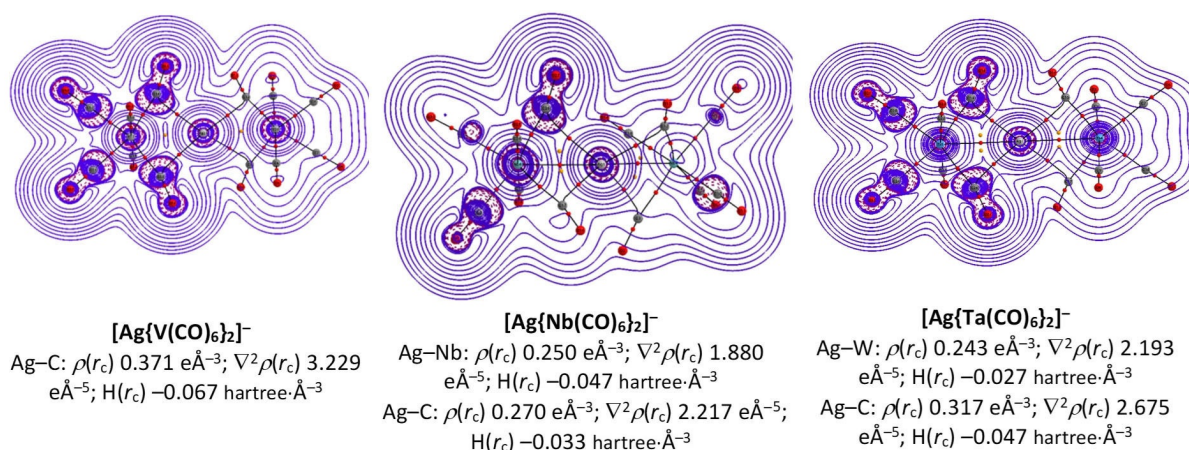
Structure and bonding within $[Ag\{M(CO)_6\}_2]^-$ (M = V, Nb, Ta)

We also calculated the group 5 hexacarbonylate complexes $[Ag\{M(CO)_6\}_2]^-$ (M = V, Nb, Ta)—as recently prepared[9] with M = Nb, Ta—and using the same methods as for the isoelectronic group 6 cations. Figure S6 (in the Supporting Information) shows the optimized geometries and the most important calculated bond lengths and angles. The complexes $[Ag\{M(CO)_6\}_2]^-$ (M = V, Ta) are predicted to have D_2 symmetric geometries, whereas the equilibrium structure of $[Ag\{Nb(CO)_6\}_2]^-$ has C_2 symmetry. All three complexes are cal-culated with two bridging CO groups for each $\{M(CO)_6\}$ ligand. The experimental structure of $[Ag\{Nb(CO)_6\}_2]^-$ also possesses two bridging CO groups with somewhat longer Ag–CO bonds than the calculated anion,[9] which are likely caused by the solid-state forces and the effect of the counterion. The experi-mental structure of $[Ag\{Ta(CO)_6\}_2]^-$ is even more complex and contains eight ions in the asymmetric unit with quite a range of slightly differing $Ag^+–[Ta(CO)_6]^-$ interactions,[9] demonstrat-ing the structural flexibility of this system.

QTAIM analysis: Figure 6 shows the contour plots of the Laplacian of the electron density, $\nabla^2\rho(r)$ of $[Ag\{M(CO)_6\}_2]^-$ (M = V, Nb, Ta) in the Ag-C-M plane, where C denotes the bridging carbonyl carbon atom of one $M(CO)_6\}_2$ moiety. The overall fea-tures are very similar as for the group 6 homologues (Figure 4). There are bond paths between the silver atom and the four bridging carbonyl carbon atoms and there are also direct bond paths for the Ag–M interactions for M = Nb, Ta, but not for M = V. The latter anion $[Ag\{V(CO)_6\}_2]^-$ has instead a ring critical point in the center of the cyclic Ag-C-V-C fragment. Interesting-ly, also the absolute magnitude of the charge densities residing on the bcps are very similar or even smaller than those within the cations. Yet, conventional wisdom would suggest that owing to the higher polarizability of the anionic ligands $[M(CO)_6]^-$, a higher charge density would be expected on the Ag–M bcps. Yet, this rationale appears to be too simple and should also be contrasted by the results of the EDA-NOCV analysis in the next section. We note that the higher magni-tude of charge density residing on the bcp does not necessari-ly imply a stronger bond.

EDA-NOCV analysis: For the EDA-NOCV analysis, it may be questioned, if the anions $[Ag\{M(CO)_6\}_2]^-$ should be discussed using Ag^+ and $[\{M(CO)_6\}_2]^{2-}$ as interacting fragments. The question can be addressed by calculations using fragments with different charges and electronic states. Those fragments, which give the smallest change in the electronic energy upon bond formation provide the best description of the moieties that give the final bond. (The best fragments for describing

[Ag{V(CO)₆}₂]⁻
Ag–C: $\rho(r_c)$ 0.371 eÅ⁻³; $\nabla^2\rho(r_c)$ 3.229 eÅ⁻⁵; $H(r_c)$ −0.067 hartree·Å⁻³

[Ag{Nb(CO)₆}₂]⁻
Ag–Nb: $\rho(r_c)$ 0.250 eÅ⁻³; $\nabla^2\rho(r_c)$ 1.880 eÅ⁻⁵; $H(r_c)$ −0.047 hartree·Å⁻³
Ag–C: $\rho(r_c)$ 0.270 eÅ⁻³; $\nabla^2\rho(r_c)$ 2.217 eÅ⁻⁵; $H(r_c)$ −0.033 hartree·Å⁻³

[Ag{Ta(CO)₆}₂]⁻
Ag–W: $\rho(r_c)$ 0.243 eÅ⁻³; $\nabla^2\rho(r_c)$ 2.193 eÅ⁻⁵; $H(r_c)$ −0.027 hartree·Å⁻³
Ag–C: $\rho(r_c)$ 0.317 eÅ⁻³; $\nabla^2\rho(r_c)$ 2.675 eÅ⁻⁵; $H(r_c)$ −0.047 hartree·Å⁻³

Figure 6. The contour plot of the Laplacian of electron density, $\nabla^2\rho(r)$ in the Ag-C-M plane of $[Ag\{M(CO)_6\}_2]^-$ (M = V, Nb, Ta). The values of topological descrip-tors are provided in au. The blue solid lines indicate regions of charge depletion ($\nabla^2\rho(r) > 0$) and red dotted lines indicate regions of charge accumulation ($\nabla^2\rho(r) < 0$). Red and yellow spheres represent bond critical points and ring critical points, respectively.

Chemistry–A European Journal

Full Paper
doi.org/10.1002/chem.202003934

Chemistry Europe
European Chemical
Societies Publishing

the final bond may not be the same as the dissociation product after bond fission. For example, the best fragments of the polar bond in LiF are the ions Li$^+$ and F$^-$ but the diatomic molecule dissociates to neutral Li and F.) It has been shown in numerous previous studies that the value for the orbital interaction ΔE_{orb} is a faithful criterion to determine the best fragments for the EDA-NOCV calculations.[25] We carried out calculations on [Ag{M(CO)$_6$}$_2$]$^-$ (M = V, Nb, Ta) with Ag^q where $q = +1$, 0, -1 and the ligands in the complementary charges. Table S3 (in the Supporting Information) gives the numerical results, which show that Ag$^+$ and {M(CO)$_6$}$_2$]$^{2-}$ as interacting fragments give the smallest ΔE_{orb} values. Therefore, we inspected the orbital terms of [Ag{M(CO)$_6$}$_2$]$^-$ (M = V, Nb, Ta) and compared them with the results for [Ag{M(CO)$_6$}$_2$]$^+$ (M = Cr, Mo, W). The numerical results of the anions are shown in Table 3. The intrinsic attraction ΔE_{int} of the group 5 complexes [Ag{M(CO)$_6$}$_2$]$^-$ (M = V, Nb, Ta) has a similar strength for the three metals. It is stronger than in the group 6 homologues [Ag{M(CO)$_6$}$_2$]$^+$ (M = Cr, Mo, W) because the hexacarbonyl ligands in the former complexes carry a negative charge, whereas they are neutral in the latter adducts. A comparison of the relative contribution of the donation and backdonation to Ag$^+$ in the group 5 anions and group 6 cations shows that the donation to the anions is only a bit stronger, whereas the contribution of the backdonation has a comparable contribution to ΔE_{orb} as the neutral species (Tables 2 and 3). The [M(CO)$_6$]$^- \rightarrow$ Ag$^+ \leftarrow$[M(CO)$_6$]$^-$ (M = V, Nb, Ta) donation amounts to 60–66% of ΔE_{orb}, whereas the backdonation [M(CO)$_6$]$^- \leftarrow$Ag$^+ \rightarrow$ [M(CO)$_6$]$^-$ provides 24–29% of the orbital interactions. The negative charge of the anionic ligands is delocalized and mainly concentrated at the electronegative oxygen atoms. This explains why the electrostatic attraction ΔE_{elstat} in the group 5 anions is only slightly stronger than in the neutral group 6 complexes (Tables 2 and 3). The deformation densities $\Delta \rho_{(1)}$–$\Delta \rho_{(9)}$ and the fragment orbitals of the group 5 com-

plexes [Ag{M(CO)$_6$}$_2$]$^-$ (M = V, Nb, Ta) are shown in Figures S7–S9 in the Supporting Information. They look very similar to the complexes of group 6 and are therefore not discussed further here. The calculated charge migration given by the eigenvalues of the deformation densities of the EDA-NOCV calculations predict a much larger donation to Ag$^+$ in the anions [Ag{M(CO)$_6$}$_2$]$^-$ (M = V, Nb, Ta) than the NBO method (Table 3), but both methods agree that the silver atom carries a positive partial charge.

Conclusion

The two novel complexes [Ag{Mo/W(CO)$_6$}$_2$][F-{Al(OR^F)$_3$}$_2$] are selectively accessible by reacting Ag[F-{Al(OR^F)$_3$}$_2$] with the respective neutral carbonyl precursor. The W system can be accessed as phase-pure crystals in good yields; the Mo system is more reactive and decomposes at room temperature. The X-ray structure of the two complexes shows that there are three carbonyl ligands from each M(CO)$_6$ fragment, which bend towards the silver atom with quite different Ag–C distances. Geometry optimizations of the free cations [Ag{M(CO)$_6$}$_2$]$^+$ (M = Cr, Mo, W) with DFT methods in the electronic singlet ground state suggest C_2-symmetric equilibrium structures with two bridging carbonyl groups for each hexacarbonyl ligand. Closely related structures are calculated for the isoelectronic group 5 anions [Ag{M(CO)$_6$}$_2$]$^-$ (M = V, Nb, Ta), which have D_2 symmetry for M = V, Ta and C_2 symmetry for M = Nb. The bonding analysis using the QTAIM method shows for all complexes bond critical points between the silver atom and the carbon atom of the bridging CO groups. Yet, there are Ag–M bond paths only for the 4d and 5d metals M, but not for the 3d atoms. In addition and somewhat unexpectedly, the absolute magnitude of the charge densities residing on the bcps is very similar for the isoelectronic anions and cations. This confirms the rather similar topology of the charge density and suggests closely related

Table 3. EDA-NOCV results for [Ag{M(CO)$_6$}$_2$]$^-$ (M = V, Nb, Ta) complexes using Ag$^+$ and {M(CO)$_6$}$_2^{2-}$ as interacting fragments at the BP86-D3(BJ)/TZ2P level. Energy values are given in kcal mol^{-1}. Calculated partial charge q(Ag) given by the NBO method and (in parentheses) the eigenvalues of the orbital interactions (see Figures S5–S7 in the Supporting Information).

Energies	Orbital interaction	[Ag]$^+$ + [V(CO)$_6$]$_2^{2-}$	[Ag]$^+$ + [Nb(CO)$_6$]$_2^{2-}$	[Ag]$^+$ + [Ta(CO)$_6$]$_2^{2-}$
ΔE_{int}		−121.5	−122.2	−122.4
ΔE_{Pauli}		148.7	149.7	164.7
ΔE_{disp}		−15.4 (3.7%)	−14.8 (3.7)	−15.3 (3.6%)
ΔE_{elstat}[a]		−269.0 (66.3%)	−256.9 (65.3%)	−285.7 (67.4%)
ΔE_{orb}[a]		−121.5 (30.0%)	−122.2 (31.0%)	−122.4 (29%)
$\Delta E_{orb(1)}$[b]	[M(CO)$_6$]$^- \rightarrow$Ag$^+$(s)$\leftarrow$[M(CO)$_6$]$^-$ σ donation	−44.4 (36.5%)	−49.1 (40.1%)	−50.0 (40.8%)
$\Delta E_{orb(2)}$[b]	[M(CO)$_6$]$^- \rightarrow$Ag$^+$(p$_\sigma$)$\leftarrow$[M(CO)$_6$]$^-$ σ donation	−15.6 (12.8%)	−17.1 (14.0%)	−17.8 (14.5%)
$\Delta E_{orb(3)}$[b]	[M(CO)$_6$]$^- \rightarrow$Ag$^+$(p$_\pi$)$\leftarrow$[M(CO)$_6$]$^-$ π donation	−6.8 (5.6%)	−7.6 (6.2%)	−7.2 (6.0%)
$\Delta E_{orb(4)}$[b]	[M(CO)$_6$]$^- \rightarrow$Ag$^+$(p$_\pi$)$\leftarrow$[M(CO)$_6$]$^-$ π donation	−5.6 (4.6%)	−6.7 (5.5%)	−5.6 (4.6%)
$\Delta E_{orb(5)}$[b]	[M(CO)$_6$]$^- \leftarrow$Ag$^+$(d$_\sigma$)$\rightarrow$[M(CO)$_6$]$^-$ σ backdonation	−5.2 (4.3%)	−5.7 (4.6%)	−6.2 (5.0%)
$\Delta E_{orb(6)}$[b]	[M(CO)$_6$]$^- \leftarrow$Ag$^+$(d$_\pi$)$\rightarrow$[M(CO)$_n$] π backdonation	−13.1 (10.8%)	−9.1 (7.4%)	−10.2 (8.3%)
$\Delta E_{orb(7)}$[b]	[M(CO)$_6$]$^- \leftarrow$Ag$^+$(d$_\pi$)$\rightarrow$[M(CO)$_6$]$^-$ π backdonation	−9.3 (7.7%)	−7.7 (6.3%)	−7.1 (5.8%)
$\Delta E_{orb(8)}$[b]	[M(CO)$_6$]$^- \leftarrow$Ag$^+$(d$_\sigma$)$\rightarrow$[M(CO)$_6$]$^-$ σ backdonation	−4.4 (3.7%)	−2.7 (2.2%)	−3.7 (3.0%)
$\Delta E_{orb(9)}$[b	[M(CO)$_6$]$^- \leftarrow$Ag$^+$(d$_\delta$)$\rightarrow$[M(CO)$_6$]$^-$ δ backdonation	−2.9 (2.4%)	−2.8 (2.3%)	−2.5 (2.0%)
$\Delta E_{orb(rest)}$[b]		−14.2 (11.6%)	−13.7 (11.2%)	−10.3 (12%)
q(Ag)		0.73 (0.18)	0.67 (0.18)	0.66 (0.18)

[a] The values in the parentheses show the contribution to the total attractive interaction $\Delta E_{elstat} + \Delta E_{orb} + \Delta E_{disp}$. [b] The values in parentheses show the contribution to the total orbital interaction ΔE_{orb}.

bonding motifs, as confirmed by the EDA-NOCV analysis. The EDA-NOCV calculations suggest that the bonding situation in the silver cations and anions can straightforwardly be described in terms of $[M(CO)_6]^q \rightarrow Ag^+ \leftarrow [M(CO)_6]^q$ donation and $[M(CO)_6]^q \leftarrow Ag^+ \rightarrow [M(CO)_6]^q$ backdonation with little impact from dispersive interactions. There are four donor components into the vacant 5s and 5p AOs of Ag^+ and five components for the backdonation from the occupied 4d AOs of the silver cation. The donation is always stronger than the backdonation, particularly in the anions. The strongest orbital interaction in all complexes is the $[M(CO)_6]^q \rightarrow Ag(s)^+ \leftarrow [M(CO)_6]^q$ donation. Importantly, donor interactions to a 5p AO of Ag^+ as acceptor apparently do play a role in the binding. Yet, the NBO method does not consider the (n)p AOs of the transition metal as genuine valence orbitals.

Experimental Section

Crystallographic data

Deposition numbers 2025554 and 2025555 contain the supplementary crystallographic data for this paper. These data are provided free of charge by the joint Cambridge Crystallographic Data Centre and Fachinformationszentrum Karlsruhe Access Structures service.

Acknowledgments

Conflict of interest

The authors declare no conflict of interest.

[1] B. Berti, M. Bortoluzzi, C. Cesari, C. Femoni, M. C. Iapalucci, R. Mazzoni, F. Vacca, S. Zacchini, *Inorg. Chem.* **2019**, *58*, 2911.

[2] V. G. Albano, L. Grossi, G. Longoni, M. Monari, S. Mulley, A. Sironi, *J. Am. Chem. Soc.* **1992**, *114*, 5708.

[3] Y.-B. Lee, W.-T. Wong, *Chem. Commun.* **2007**, 3924.

[4] J. Zhang, L. F. Dahl, *J. Chem. Soc. Dalton Trans.* **2002**, 1269.

[5] P. Klüfers, *Z. Krist. Cryst. Mater.* **1984**, *166*, 143.

[6] G. Wang, Y. S. Ceylan, T. R. Cundari, H. V. R. Dias, *J. Am. Chem. Soc.* **2017**, *139*, 14292.

[7] P. J. Malinowski, I. Krossing, *Angew. Chem. Int. Ed.* **2014**, *53*, 13460; *Angew. Chem.* **2014**, *126*, 13678.

[8] W. Unkrig, M. Schmitt, D. Kratzert, D. Himmel, I. Krossing, *Nature Chem.* **2020**, *12*, 647.

[9] W. Unkrig, K. Kloiber, I. Krossing, B. Butschke, D. Kratzert, *Chem. Eur. J.* **2020**, *26*, 12373.

[10] a) S. C. Meier, D. Himmel, I. Krossing, *Chem. Eur. J.* **2018**, *24*, 19348; b) S. C. Meier, A. Holz, J. Kulenkampff, A. Schmidt, D. Kratzert, D. Himmel, D. Schmitz, E.-W. Scheidt, W. Scherer, C. Bülow, M. Timm, R. Lindblad, S. T. Akin, V. Zamudio-Bayer, B. von Issendorff, M. A. Duncan, J. T. Lau, I. Krossing, *Angew. Chem. Int. Ed.* **2018**, *57*, 9310; *Angew. Chem.* **2018**, *130*, 9454; c) S. C. Meier, A. Holz, A. Schmidt, D. Kratzert, D. Himmel, I. Krossing, *Chem. Eur. J.* **2017**, *23*, 14658.

[11] J. Bohnenberger, W. Feuerstein, D. Himmel, M. Daub, F. Breher, I. Krossing, *Nat. Commun.* **2019**, *10*, 624.

[12] J. Bohnenberger, B. Derstine, M. Daub, I. Krossing, *Angew. Chem. Int. Ed.* **2019**, *58*, 9586; *Angew. Chem.* **2019**, *131*, 9687.

[13] J. Bohnenberger, I. Krossing, *Angew. Chem. Int. Ed.* **2020**, *59*, 5581; *Angew. Chem.* **2020**, *132*, 5629.

[14] I. M. Riddlestone, A. Kraft, J. Schaefer, I. Krossing, *Angew. Chem. Int. Ed.* **2018**, *57*, 13982; *Angew. Chem.* **2018**, *130*, 14178.

[15] I. Krossing, *Chem. Eur. J.* **2001**, *7*, 490.

[16] A. Martens, P. Weis, M. C. Krummer, M. Kreuzer, A. Meierhöfer, S. C. Meier, J. Bohnenberger, H. Scherer, I. Riddlestone, I. Krossing, *Chem. Sci.* **2018**, *9*, 7058.

[17] J. Bohnenberger, M. Schmitt, W. Feuerstein, I. Krummenacher, B. Butschke, J. Czajka, P. J. Malinowski, F. Breher, I. Krossing, *Chem. Sci.* **2020**, *11*, 3592.

[18] T. C. W. Mak, *Z. Kristallogr. Cryst. Mater.* **1984**, *166*, 277–281.

[19] F.-W. Grevels, J. Jacke, W. E. Klotzbücher, F. Mark, V. Skibbe, K. Schaffner, K. Angermund, C. Krüger, C. W. Lehmann, S. Özkar, *Organometallics* **1999**, *18*, 3278.

[20] R. F. W. Bader, *Atoms in Molecules: A Quantum Theory*, Clarendon, Oxford, **2003**.

[21] G. Frenking, N. Fröhlich, *Chem. Rev.* **2000**, *100*, 717.

[22] a) C. Foroutan-Nejad, S. Shahbazian, R. Marek, *Chem. Eur. J.* **2014**, *20*, 10140; b) R. F. W. Bader, *J. Phys. Chem. A* **2009**, *113*, 10391.

[23] a) L. Zhao, M. Hermann, W. H. E. Schwarz, G. Frenking, *Nat. Rev. Chem.* **2019**, *3*, 48; b) L. Zhao, M. von Hopffgarten, D. M. Andrada, G. Frenking, *WIREs Comput. Mol. Sci.* **2018**, *8*, e1345; c) A. Michalak, M. Mitoraj, T. Ziegler, *J. Phys. Chem. A* **2008**, *112*, 1933; d) M. P. Mitoraj, A. Michalak, T. Ziegler, *J. Chem. Theory Comput.* **2009**, *5*, 962.

[24] F. Weinhold, C. Landis, *Valency and Bonding, A Natural Bond Orbital Donor–Acceptor Perspective*, Cambridge University Press, Cambridge, **2005**.

[25] a) Q. Wang, S. Pan, Y.-B. Wu, G. Deng, J.-H. Bian, G. Wang, L. Zhao, M. Zhou, G. Frenking, *Angew. Chem. Int. Ed.* **2019**, *58*, 17365; *Angew. Chem.* **2019**, *131*, 17526; b) R. Saha, S. Pan, G. Merino, P. K. Chattaraj, *Angew. Chem. Int. Ed.* **2019**, *58*, 8372; *Angew. Chem.* **2019**, *131*, 17848; c) D. M. Andrada, J. L. Casals-Sainz, Á. Martín Pendás, G. Frenking, *Chem. Eur. J.* **2018**, *24*, 9083; d) Z. Wu, J. Xu, L. Sokolenko, Y. L. Yagupolskii, R. Feng, Q. Liu, Y. Lu, L. Zhao, I. Fernández, G. Frenking, T. Trabelsi, J. S. Francisco, X. Zeng, *Chem. Eur. J.* **2017**, *23*, 16566; e) D. C. Georgiou, L. Zhao, D. J. D. Wilson, G. Frenking, J. L. Dutton, *Chem. Eur. J.* **2017**, *23*, 2926; f) L. T. Scharf, D. M. Andrada, G. Frenking, V. H. Gessner, *Chem. Eur. J.* **2017**, *23*, 4422.